GA-A20273

DIII-D RESEARCH PROGRAM PROGRESS

by
R.D. STAMBAUGH and the DIII-D TEAM

NOVEMBER 1990

GENERAL ATOMICS

DISCLAIMER

GA-A--20273

DE91 006409

DIII-D RESEARCH PROGRAM PROGRESS

by
R.D. STAMBAUGH and the DIII-D TEAM

This is a preprint of a paper to be presented at the Thirteenth International Conference on Plasma Physics and Controlled Nuclear Fusion Research, October 1–6, 1990, Washington, DC, and to be printed in the *Proceedings*.

Work supported by
U.S. Department of Energy
Contract DE-AC03-89ER51114

GENERAL ATOMICS PROJECT 3466
NOVEMBER 1990

GENERAL ATOMICS

IAEA CN–53/A–1–4

DIII–D RESEARCH PROGRAM PROGRESS*

ABSTRACT

A summary of highlights of the research on the DIII–D tokamak in the last two years is given. At low q, toroidal beta (β_T) has reached 11%. At high q, $\epsilon\beta_p$ has reached 1.8. DIII–D data extending from one regime to the other show the beta limit is at least $\beta_T(\%) \geq 3.5\ I/aB$ (MA, m, T). Prospects for using H–mode in future devices have been enhanced. The discovery of negative edge electric fields and associated turbulence suppression have become part of an emerging theory of H–mode. Long pulse (10 second) H–mode with impurity control has been demonstrated. Radial sweeping of the divertor strike points and gas puffing under the X–point have lowered peak divertor plate heat fluxes a factor of 3 and 2 respectively. $T_i = 17$ keV has been reached in a hot ion H–mode. Electron cyclotron current drive (ECCD) has produced up to 70 kA of driven current. Program elements now beginning are fast wave current drive (FWCD) and an advanced divertor program (ADP).

1. INTRODUCTION

The DIII–D research program has as its long range goal the integrated demonstration of high β operation with good confinement and non-inductive current drive to provide a basis for tokamak progress toward steady-state reactors. This goal is pursued through several lines of research which are also important for their contributions to basic tokamak physics. We describe these areas and recent research accomplishments in them.

Plasma cross-section shaping and profile control are employed to probe β limits and increase β. Recently in the low q regime $q_{95} \sim 2.6$, $\beta_T = 11\%$ in a highly elongated ($\kappa = 2.35$) double-null divertor plasma was achieved [1], demonstrating the tokamak can sustain β considerably in excess of that planned in future devices. The β_T part of the integrated demonstration referred to above has been met with $\beta_T = 5\%$ reached at

*This is a report of work sponsored by the Department of Energy under Contract No. DE-AC03-89ER51114.

full $B_T = 2.1$ T [2]. The scaling of β, β_T (%) $\geq 3.5\ I/aB$ (MA, m, T), and detailed analyses continue to be well in accord with theory, laying a solid foundation for future device design [2,3]. At higher q, the normalized beta, $\beta_N \equiv \beta_T/(I/aB)$, has reached 5 [2,3] and at still higher q, $\beta_p = 5.1$ and $\epsilon\beta_p = 1.8$ have been reached [4]. These results, achieved in the regime where bootstrap current can be large, are favorable for current driven reactor designs [5].

For enhanced confinement, DIII–D contributes to providing a basis for the use of H–mode in future devices [6]. A scaling for ELM-free H–mode confinement was worked out by a joint team from JET and DIII–D [7]. Considerable progress was made on elucidating the physics basis of H–mode. A sudden increase in edge poloidal rotation, corresponding to an increased negative edge electric field was discovered on DIII–D [8]. Subsequently detailed investigations have not conclusively shown edge rotational effects cause the L-H transition [9], but substantial evidence points to increased shear in edge rotation as the mechanism for edge turbulence suppression [10]. H–mode with flat density profiles has been shown able to sustain a hot ion regime; $T_i = 17$ keV has been reached [11]. Theory suggests two fundamental prescriptions for scaling confinement results to future devices, the Bohm or gyro-Bohm prescriptions depending on whether the turbulence is long scale (a) or short scale (ρ_S) respectively. An experiment comparing dimensionally similar discharges was done to distinguish between these two possibilities [12]; the gyro-Bohm model is favored.

For long pulse impurity control and heat flux handling, two important results were obtained. A 10 sec long nearly stationary H–mode [13], was produced by using ELMs to control impurity levels [14]. Two methods, radial sweeping of the divertor strike points and gas puffing under the X–point to encourage a radiative divertor plasma, were each shown able to lower time average peak heat fluxes a factor of 3 and 2 respectively [15]. These methods could be applied in combination.

For non-inductive current drive, two rf methods are being developed: electron cyclotron current drive (ECCD) and fast wave current drive (FWCD). A first result, up to 70 kA of driven current, has been produced using 1 MW of 60 GHz (fundamental) waves launched in X–mode from the inboard side [16]. The rf program also seeks to develop ECH as a heating tool; important transport results, ELM suppression studies, and H–mode studies have been carried out [17]. Near term plans call for ECH to provide some current drive and also the high T_e regime in which FWCD can be efficient.

2. RECENT MODIFICATIONS

In the last two years, the following facility modifications, which are important in the results to be described, were implemented.

1. *Neutron Shielding* was added around the entire DIII-D machine pit. The resulting shielding factor of 300 allowed routine $D^\circ \rightarrow D^+$ operation. The improved confinement from the isotope dependence $\tau_E \sim \sqrt{M_i}$ was important in reaching high beta and high performance plasmas.

2. *Deuterium Neutral Beam Operation* enabled the output power of the four beamline system to be increased from 14 MW H° to 20 MW D°, also an important factor in attaining higher beta and stored energy.

3. *Carbonization* of the vacuum vessel wall (half graphite and half Inconel) was done by means of a glow discharge in a mixture of helium and deuterated methane. Subsequent glow in pure helium was used to desorb deuterium from the carbon film. The result was a reduction in metallic impurity levels by a factor of 30. The carbonization enabled an increase in the plasma current at which we could reliably operate divertor discharges from 2 MA to 3 MA with H-mode, an increase in the peak achieved stored energy from 2.6 MJ to 3.6 MJ, and an increase in the ion temperature from 11 to 14 keV in hot ion H-mode in corresponding conditions. Peaked density profiles ($n(0)/\bar{n}_e = 2$) were produced in H-mode and the ELM frequency was doubled [18].

4. *Ion Bernstein Wave Heating* (IBW) was initiated to get a local ion heating system for manipulation of H-mode plasmas that potentially did not produce ion tails and avoided the loading problems with fast waves and H-mode [19]. A 30–60 MHz, 2 MW generator feeding a pair of cavity type end fed loop antennas oriented along the toroidal field was used. Unfortunately, central ion heating was never seen and the loading (~5 Ohms) was one to two orders of magnitude greater than theoretical prediction and never displayed any of the expected resonances at ion cyclotron harmonics. Edge electron heating was observed. Edge ion heating was correlated with increased amplitudes of parametric decay spectra. Impurity influx was customary, except with carbonization. This program has been discontinued.

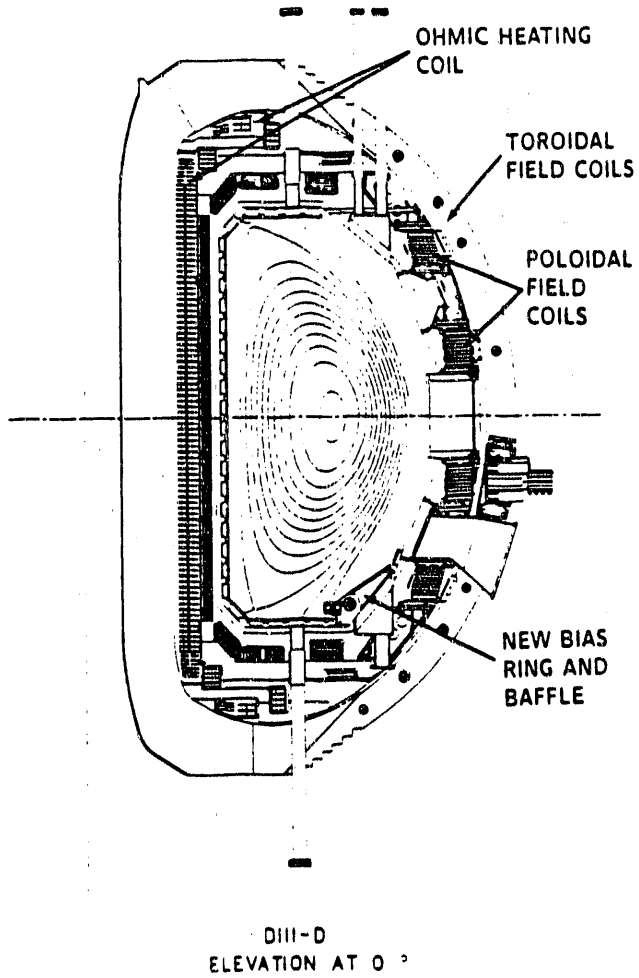

Fig. 1. Cross section of DIII–D. The equilibrium is from the 11% β_T discharge. The divertor ring has only just been installed.

5. A four strap fast wave current drive antenna has been installed in place of the IBW antenna. It is designed to handle 4 MW; the 2 MW generator will be used in initial tests of heating and current drive.

6. A baffle and ring electrode structure has recently been installed (Fig. 1) to enable particle and energy confinement experiments with divertor biasing and pumping.

3. HIGH TOROIDAL BETA β_T AND NORMALIZED BETA β_N

The situation in regard to maximal β_T limits is summarized in Fig. 2. Certainly the envelope of the data supports the conclusion that the beta

limit is at least as high as $\beta_N = 3.5$; however, this conclusion is couched as an "at least" statement because the achieved β_T in most cases on this plot was limited by the product of available heating power and confinement time ($W = \mathrm{P} \times \tau_E$) rather than disruptive instabilities. Discharges identified as large open circles have been identified as clear candidates for external kink disruptions as evidenced by the m/n = 2/1 locked mode precursor with fast growth time. Wall stabilization should be ineffective for locked modes (merely limiting the growth time to the vessel wall time constant, ~3 msec in DIII–D) and so it is not surprising that our low-n mode stability calculations agree with those of Troyon on a limiting $\beta_N = 2.8$ in these cases of free boundary kinks with no wall stabilization [20]. For a conducting wall at $1.5a$ from the plasma surface and nominal profiles, we find the low-n ideal limit at about $\beta_N = 4$ [2,21].

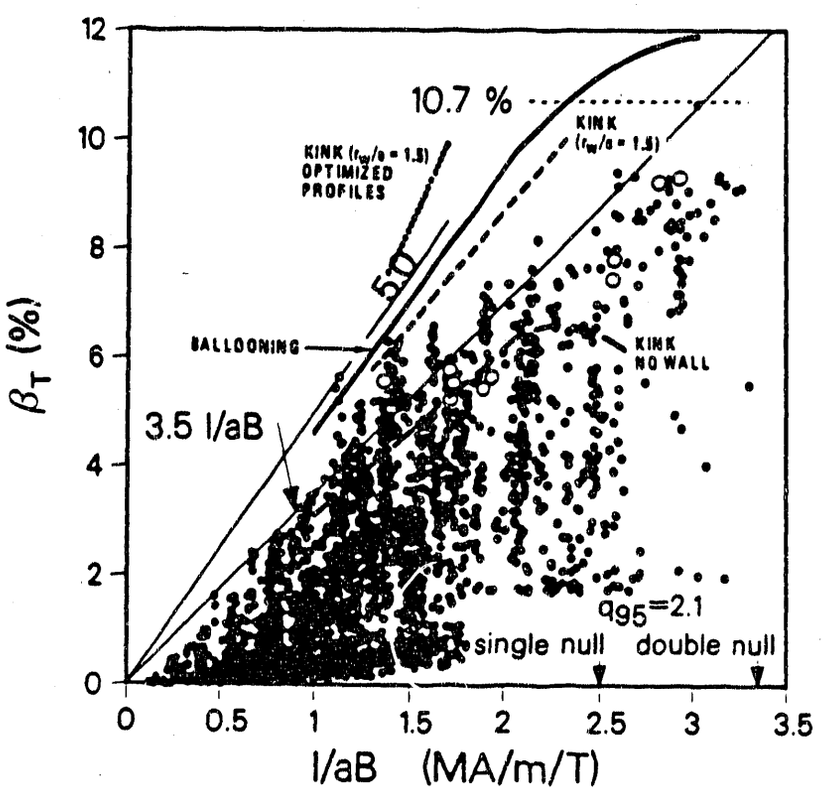

Fig. 2. Equilibrium fit β versus I/aB for DIII–D. The lines at $\beta_T = 3.5$ (5.0) I/aB are to guide the eye. The open circles locate ideal time-scale $m/n = 2/1$ disruptions. Various β-limit calculations are summarized in the curves (———, – –, - - -, . . .) with differing assumptions on the location of a conducting wall (r_w/a).

Recently we have found that if in addition to the nearby conducting wall, profiles are optimized, the low-n limit can be raised to $\beta_N \sim 5.5$ [22]. This possibility was first made clear in the calculations shown in Fig. 3. For broader pressure profiles, but more peaked current profiles ($\ell_i \sim 0.93$), access to $\beta_N \sim 5.5$ was predicted for $q_{95} = 3.2$ and $q_0 = 1.05$. Quite independently, an experimental campaign succeeded in producing stable discharges at $\beta_N = 5.0$ at about $I_N = I/aB = 1$–1.5 ($q_{95} \sim 4$–5) as shown in Fig. 2. Stability calculations at that q value (4–5) [2] also predict an optimized profile path to low-n ideal stability and so we have drawn the short curve segment in the figure representing our calculated low-n stability limit with optimized profiles. Further calculations are needed to see the range of I_N for which $\beta_N \sim 5.5$ can be stable. For high-n modes, our ideal MHD calculations in the ballooning representation have predicted an optimized profile limit of $\beta_N \sim 4.5$ [21], in good agreement with Sykes' result [23]. It remains to be seen whether these high values of β_N can be reached over a broad range of I/aB and so redefine the expected beta limit up to $\beta_N \sim 5$. Such an outcome could be important since it may allow future devices to be designed for operation at $\beta_N \sim 3.5$ [5] instead of the now customary cautious choice of $\beta_N \sim 2$.

With a beta limit scaling of the form $\beta_N \leq$ constant, the task of maximizing the absolute value of β_T becomes that of maximizing the normalized plasma current I_N subject to the constraint $q_{95} > 2$ and providing sufficient power and confinement time. Using single-null divertor plasmas a maximum I/aB = 2.3 was reached and a maximum $\beta_T = 7.4\%$. Double-null discharges allowed about the largest divertor plasma cross-section that would fit in the vacuum chamber and increased triangularity which allowed a larger I/aB = 3.3 and a maximum β_T of 9.3%. This 9.3% value was reached in a 60 msec long ELM-free phase following the L-H transition and the subsequent ELMs clamped β_T to 8% for 0.9 seconds [2].

4. HIGH ELONGATION AND HIGHEST β_T

Since the largest cross-section plasma in DIII–D has $\kappa \sim 2$, in order to further increase I/aB, it was necessary to decrease a in order to increase κ. Studies of the axisymmetric stability limits in DIII–D found that the ideal axisymmetric limits coincided with the predictions of GATO to within a few percent [24]. Between $\kappa = 2$ and 2.5, the simple rigid body shift model (m = 1) becomes inadequate and both the experiment and the calculations show that the vertical stability limit at $\kappa \sim 2.5$ has a large m/n = 3/0 component in the plasma motion. It was found that coils near the inboard midplane are optimal for vertical feedback control,

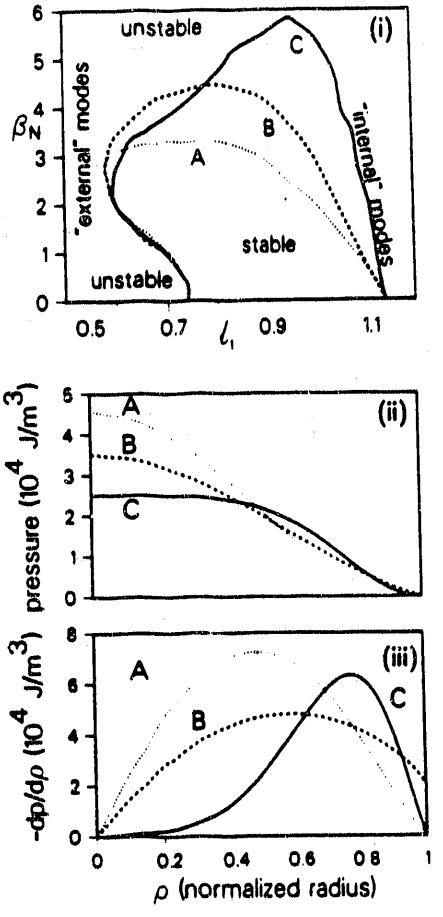

Fig. 3. The calculated ideal, $n = 1$ mode stability boundaries (i) versus internal inductance ℓ_i for the pressure (ii) and pressure gradient profiles (iii) shown versus normed volume radius ρ. Mode displacement vectors peak near the edge for "external" modes and near the center for "internal" modes.

since they have minimal interaction with the passive image current flow patterns in the vacuum vessel which dominate the vertical stability [24]. The principal importance of these studies was close (within a few percent) agreement between experimentally observed vertical stability limits and theoretically predicted limits (GATO).

With this basis of understanding and control system improvements, plasmas with $a = 0.56$ m and $\kappa = 2.35$ were operated at low $B_T = 0.75$ T to assess their β capability. With $P_{NBI} = 19$ MW, $\beta_T = 11\%$ was reached [1]. Plasma current was 1.29 MA; I/aB = 3.1 and $q_{95} = 2.56$. The equilibrium for this discharge is shown in Fig. 1. Various measures of β_T were equilibrium fitting (10.7%), diamagnetism (10.8%), and kinetic profile integration with the fast ion contribution computed by standard methods (11.3%). Besides the higher NBI power, the proximate cause why this

discharge reached such high beta seems to have been the absence of sawteeth on the beta rise. Kinetic profile data show the thermal beta on axis to be 20%; standard beam deposition codes estimate the fast ion beta on axis to be an additional 20%. These results raise the issues of FLR effects and fast ion stabilization of interior modes, subjects of current investigation. However, this result does establish that the tokamak can contain an absolute value of β_T (11%) much in excess of that planned in CIT and ITER ($\beta_T \sim$ 4%–6%).

5. ATTACHED EQUILIBRIA

Vertical instabilities in highly elongated plasmas have produced very large forces on the vacuum vessel in DIII–D and JET. The vertically unstable plasma drifts down at a speed limited by vessel image currents, limiting on the bottom of the vessel and shrinking in cross-section until it disrupts. We have found that while drifting the equilibria are "attached" to the vessel in the sense shown in Fig. 4. In a 1 MA discharge up to 0.3 MA flows on the open field lines, outside the last closed flux surface, completing the circuit through the bottom of the vacuum vessel. These attached currents have been detected both by equilibrium fitting of magnetic data and directly by the resistive shunts under the divertor tiles and divertor tile Rogowski coils with excellent agreement between the two methods. The force arising from the poloidal component of this current crossed with B_T accounts for the observed up/down motion of the vacuum vessel [14]. Such large wall currents must be carefully considered in future machine designs.

6. HIGH BETA POLOIDAL

Probing for the possible existence of a second stable regime, at very high q (q_{95} = 18, I = 0.54 MA, at B_T = 2.1 T), 14 MW NBI was used to produce the very high value of $\beta_p = 5.1$ and $\epsilon\beta_P = 1.8$ [4]. These plasmas are approaching the equilibrium limit, with a magnetic axis shift of 0.22 m out of a = 0.61 m equal to the inverse aspect ratio 0.36 and the poloidal field on the inboard side weakened to 1/3 of the value on the outboard side. The high β_p and confinement equal to 2.3 × ITERP-89 are realized during the ELM-free phase. During ELMs, confinement is reduced and $\epsilon\beta_P$ was maintained near 1.0. High-n stability calculations show, as was the case for previous results along this line [25], that with the

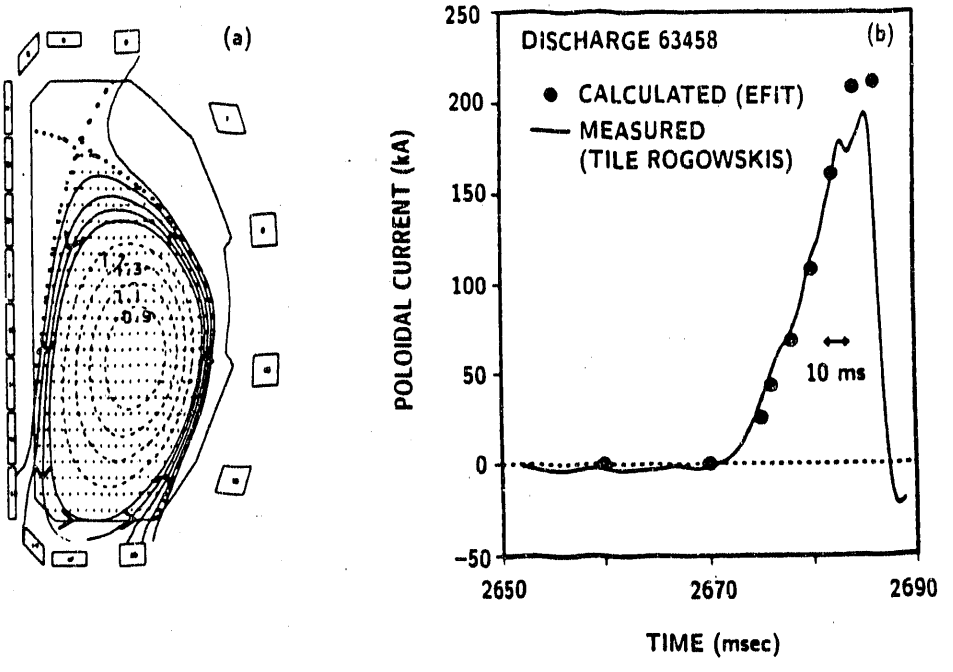

Fig. 4. "Attached" equilibrium (a) during a vertical instability prior to the disruption. Arrows show the poloidal direction of flow of currents flowing partly in the scrape-off layer and partly in the vacuum vessel wall. Directly measured currents into divertor tiles agree with currents inferred from equilibrium fitting (b).

motional Stark effect measured $q_0 = 1.3$–2.0, most of the plasma cross-section, except the very center, is in the transition region from first to second stability.

7. CONFINEMENT SCALING

In the last two years, JET and DIII-D carried out a joint program of H-mode confinement scaling studies aimed at discovering the dependence on machine size [7]. Both devices operated carefully designed single-null divertor plasmas with the same shape ($\kappa = 1.8$) and toroidal field (2–2.5 T). Confinement was studied in the ELM-free phase to avoid difficult to quantify effects of ELMs on confinement. Because both machines have the same aspect ratio 2.7, separate dependences on a and R were not

determinable, the result is quoted in terms of a choice of linear dimension. Dimensionally correct scalings are discussed in Ref. 7. In engineering variables, the result is

$$\tau_E(\mathrm{sec}) = C\, I_p^{1.03\pm0.07}\, P_L^{-0.46\pm0.06}\, L^{1.48\pm0.09}\ (\mathrm{MA, MW, m}) \quad ,$$

$$C = 0.106 \pm 0.011 \text{ for } L = R$$
$$= 0.441 \pm 0.044 \text{ for } L = a \quad .$$

In another approach to deducing fundamental aspects of transport scaling, it has been shown that almost all magnetized plasma diffusion mechanisms can be cast in the form of a gyro-Bohm (gB) or Bohm (B) scaling, depending on whether the normative length scale in the problem is the short length ρ_S or the long length a respectively [12]. Local diffusivities can be written as $\chi_{gB} = (c_S/a)\rho_S^2 F_{gB}$ or $\chi_B = c_S \rho_S F_B$, the form factors F depending only on dimensionless parameters. Any two discharges for which the dimensionless parameters are the same, and therefore F, are said to be dimensionally similar and in that case one should observe either the local scaling $\chi_{gB} \propto B^{-1} a^{-1/2}$ or $\chi_B \propto B^{-1/3} a^{1/3}$. Two dimensionally similar L–mode discharges were constructed in DIII–D with $a = 0.65$ m, $A = 2.7$, $\kappa = 1.70$, $q_{95} = 3.8$, the same $\beta = 1.96\% \pm 0.03\%$, and the same $\nu_{*e}^{\mathrm{MIN}} = 0.128 \pm 0.001$, but varying B = 1.05 T (1 MA) to B = 2.1 T (2 MA). The experimental results of local transport analyses for a single fluid χ are given as the smooth curves in Fig. 5. The curves given by symbols are the predictions of the 2 T result based on scaling the 1 T result according to either the gyro-Bohm or Bohm prescriptions. The gyro-Bohm scaling is in better agreement with the experimental result at 2 T than the Bohm scaling.

8. HOT ION H–MODE

At modest currents (~1 MA) and with helium glow wall conditioning, it is possible to keep the Ohmic plasma density low, ~1×10^{19} m^3. The application of strong beam heating results in a prompt L-H transition. In the subsequent long ELM-free period, although the density is rising, it remains low enough that electron-ion coupling is not large and the ion temperature readily pulls away from the electron temperature. In this hot ion H–mode regime, $T_i(0)$ as high as 17 keV has been reached; profiles for that discharge are in Fig. 6. The hot ion H–mode has produced

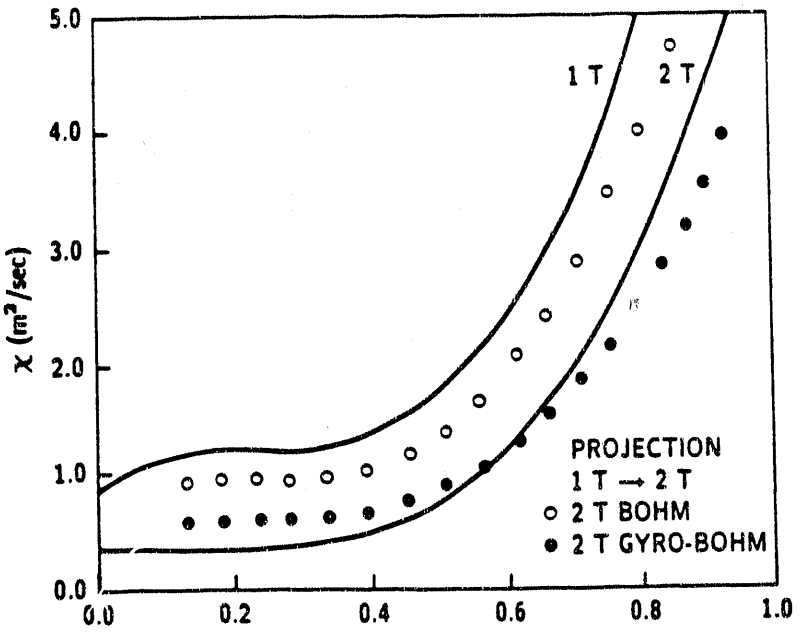

Fig. 5. The solid lines are the single fluid diffusivities calculated from experimental data versus normed volume radius ρ for $B = 1$ T and 2 T dimensionally similar plasmas. Based on the 1 T result, the predicted 2 T result for Bohm (o) and gyro-Bohm (•) scaling.

the highest DD neutron rate of 2.7×10^{15}/sec corresponding to $Q_{DD} = 0.00026$.

In going from similar limiter L–mode discharges to hot-ion H–mode discharges, transport analysis showed [11]:

1. χ_e improves the most, about a factor of three;
2. χ_ϕ and χ_e improve equally and are about equal for $\rho > 0.3$;
3. χ_i improves only inside $\rho < 0.5$;
4. χ_i is significantly less than χ_e inside $\rho = 0.5$ and is within error bars of neoclassical.

9. L-H TRANSITION PHYSICS

Besides the usual H_α drop, two additional clear signatures of H–mode were found, an abrupt increase in edge plasma poloidal rotation speed and an abrupt drop in edge plasma turbulence levels (Fig. 7) [26,27]. The drop in turbulence levels occurs within 100 microseconds of the transition

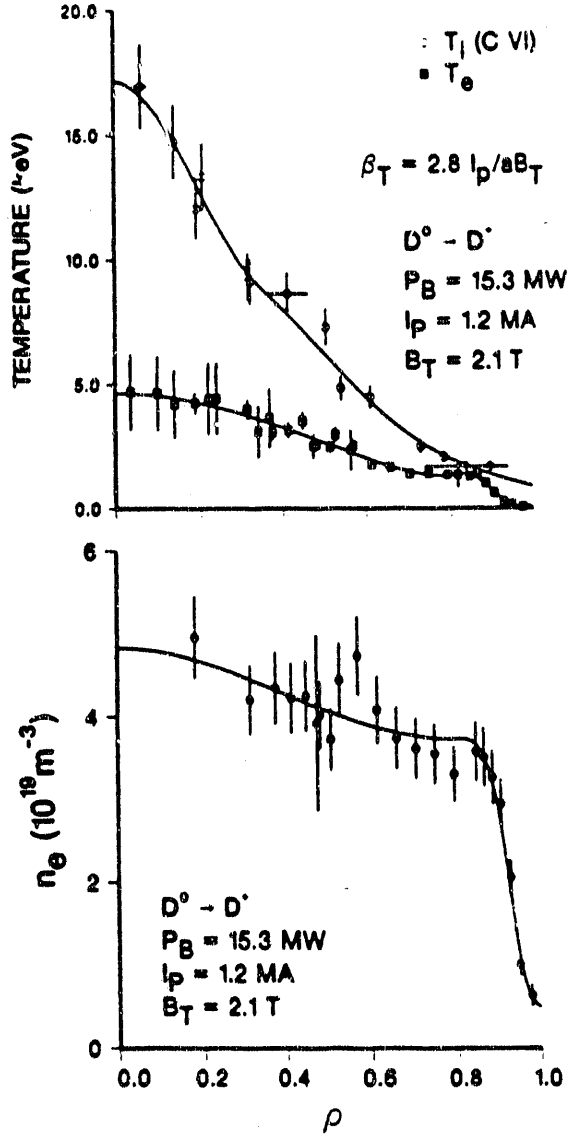

Fig. 6. Ion and electron temperature and electron density profiles in the highest T_i, hot-ion H-mode discharge.

and is seen in both magnetic fluctuations and density fluctuations detected by a microwave reflectometer system [28]. The change in poloidal rotation speed ($v_p \times B_T$ term) is the dominant factor in an increasingly negative radial electric field via the force balance equation [8]: $E_r = \frac{1}{n_i Z_i e} \nabla P_i - (\vec{V}_i \times \vec{B})_r$ (Fig. 7). The theory of Shaing [9] suggests the sudden increase in rotation speed arises from a bifurcation in the poloidal flow equation in which edge ion orbit loss is the mechanism to charge the

plasma negatively; in which case the enhanced rotation should penetrate a few poloidal ion Larmor radii into the plasma. These observations also prompted the theory suggestion that shear in rotation could suppress turbulence by shearing apart turbulent eddies [10]; in which case one expects overlap between the region of enhanced shear and turbulence suppression. We upgraded our edge Charge Exchange Recombination system to provide 1.5 cm edge spatial resolution and added a continuously variable frequency reflectometer system to make detailed edge measurements. Results to date show good agreement between the location of the rotational shear layer and the zone of improved confinement [29]. On the question of causality, we have some cases where the rotation change begins a few msec before the L-H transition, but no cases in which the rotation change follows the edge turbulence drop.

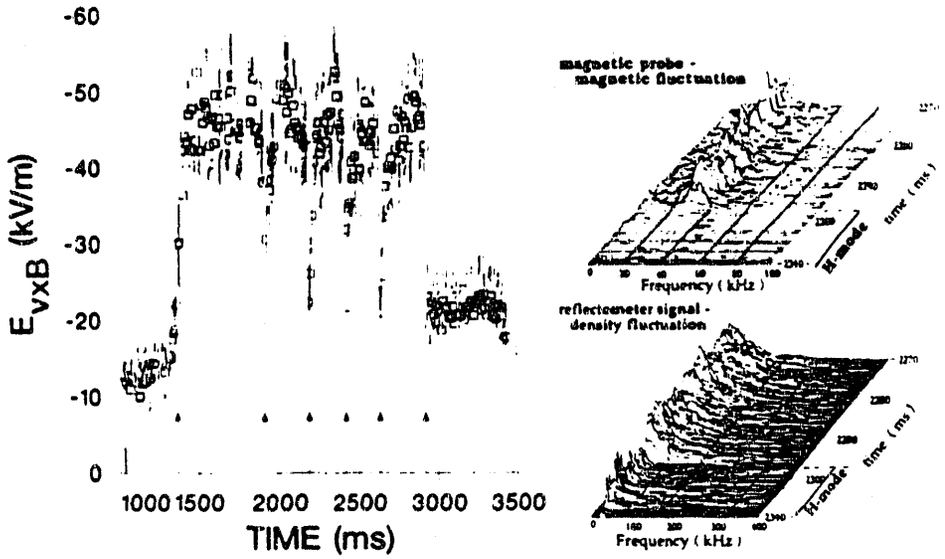

Fig. 7. Dominant $\vec{v} \times \vec{B}$ term in the radial electric field becomes more negative at L-H transition ($t = 1500$ msec) and less negative at each ELM (arrows). Magnetic and density fluctuations drop abruptly in H-mode.

10. EDGE LOCALIZED MODES (ELMs)

Three kinds of ELMs have been identified on DIII-D, presented in reverse order of their identification as a sub-species but in increasing order of the severity of their effects on the discharge. The existence of different

types of ELMs has complicated our studies of whether ELMs are primarily pressure or current driven instabilities.

Type III. These are small amplitude ELMs which occur when the NBI power is just above threshold. As the power is increased, their frequency decreases and they disappear. The edge pressure gradient for Type III ELMs is well below the $n = \infty$ ideal ballooning limit.

Type II. These are high frequency, low amplitude ELMs which appear when the edge plasma region is put into the connection region between the first and second stable ballooning regimes by increased elongation and/or triangularity in low to moderate current plasmas ($I_p/B_T < 0.5$) [30].

Type I. Popularly called "giant ELMs," these play the major role in H–mode discharges. The edge pressure gradient prior to these ELMs is consistently at the ballooning limit [31]. Their frequency (f) increases with power and decreases as current is raised [32]. We have also found that ECH applied at the plasma edge can significantly affect the ELM frequency [17]. The role of ELMs in confinement is still a subject of controversy. In many discharges, a brisk rise in stored energy in the ELM-free phase appears to be completely arrested by the first ELM, implying the ELMs play a dominant role in H–mode confinement [33]. However, diamagnetic loop measurements show that the energy loss per ELM (δE) decreases with power and increases with current such that the ELM power $= f \times \delta E$ is roughly constant at a low level 0.5–1.0 MW compared to input power >4 MW. These results were confirmed in a few cases by infrared TV measurements at the divertor plate [15].

11. TEN SECOND H–MODE

The efficacy of giant ELMs in conjunction with flat to hollow density profiles in preventing impurity accumulation has been well documented [34]. The ELM frequency can be continuously adjusted through plasma shape, current, and input power. An outstanding example is the 10 second long H–mode in Fig. 8; impurity levels are decreasing slowly in time [14]. The confinement enhancement over ITERP-89 is 1.4 at late times in the discharge when the ELM frequency is high, compared to an average enhancement factor of 1.7 for the DIII–D data in the ITER H–mode data base. The density is rising at a rate about 1/10 of the

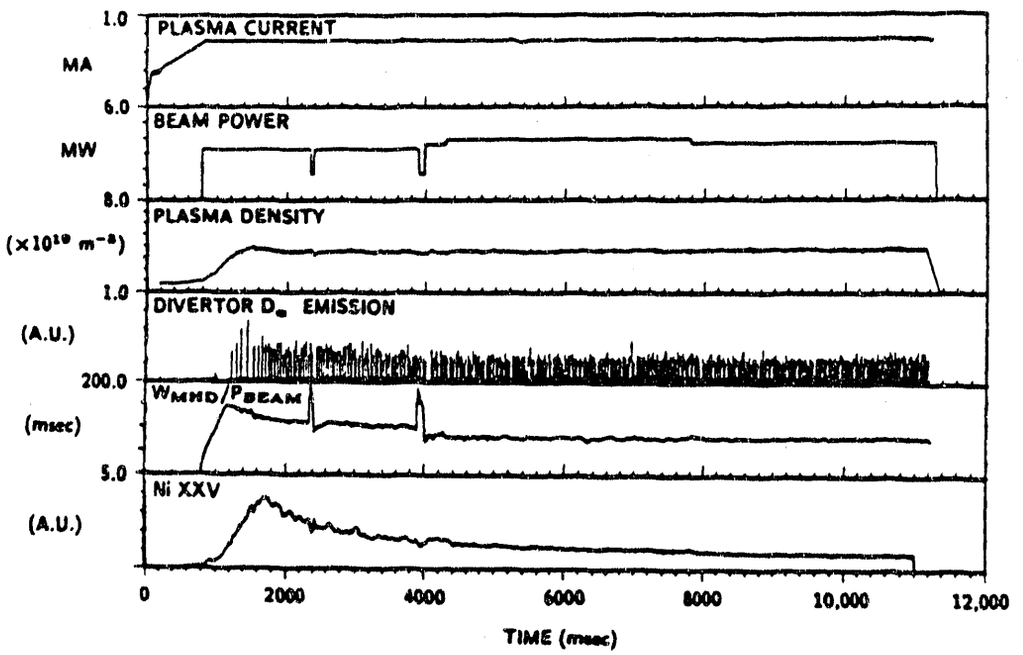

Fig. 8. Ten second H–mode impurity control via ELMs.

NBI particle input rate, indicating substantial particle absorption into the graphite.

12. HIGH RECYCLING DIVERTOR

Previous studies [35,36] have shown that the DIII–D divertor plasma operates in the high recycling regime (ion flux at the divertor plate/ion flux out of the core plasma > 10, $n_{e,div} > n_{e,sep}$, and $T_{e,div} < T_{e,sep}$). Recent B2 code modelling agrees with previous ONETWO/DEGAS modelling that the density evolution in H–mode requires an inward pinch term and a ratio of $D/V \sim 0.05$ m. The strong density rise in H–mode is accounted for by a factor of 2 improvement in τ_p but also by about a factor of 2 increase in the core plasma fueling rate. DEGAS calculations show this surprising result to arise from a factor of 2 reduction in divertor recycling flux being overcome by about a factor of 3-4 increase in the penetration of neutrals through the scrape-off layer because that layer is much thinner in H–mode compared to L–mode [36].

13. RADIATIVE DIVERTOR AND X–POINT SWEEPING

The high local heat fluxes at the separatrix strike points are difficult design issues in CIT and ITER. Previously, we had shown that the X–point could be swept sufficiently to lower the peak heat flux by a factor of 3 without affecting other aspects of the plasma operation. The ±6 cm sweeping heat flux pattern on the divertor plates as viewed from above by an IR camera is shown in Fig. 9(b). Recently, we have employed gas puffing in the region between the separatrix strike points to make the divertor plasma more radiative. Deuterium gas injected at a rate of 120 torr l/sec into a discharge with 14.5 MW NBI lowered the peak heat flux from 4 MW/m^2 to 2 MW/m^2 [Fig. 9(a)] with very little other effect on the plasma. Nitrogen injection was also fairly successful. With 20 MW NBI, the nitrogen injection reduced the target heat flux from 3 MW/m^2 to less than 1.5 MW/m^2 with only a 5%–15% drop in τ_E and Z_{eff} increasing from 1.8 to 2.4 [15]. The combination of the radiative divertor and X–point sweeping is no doubt possible.

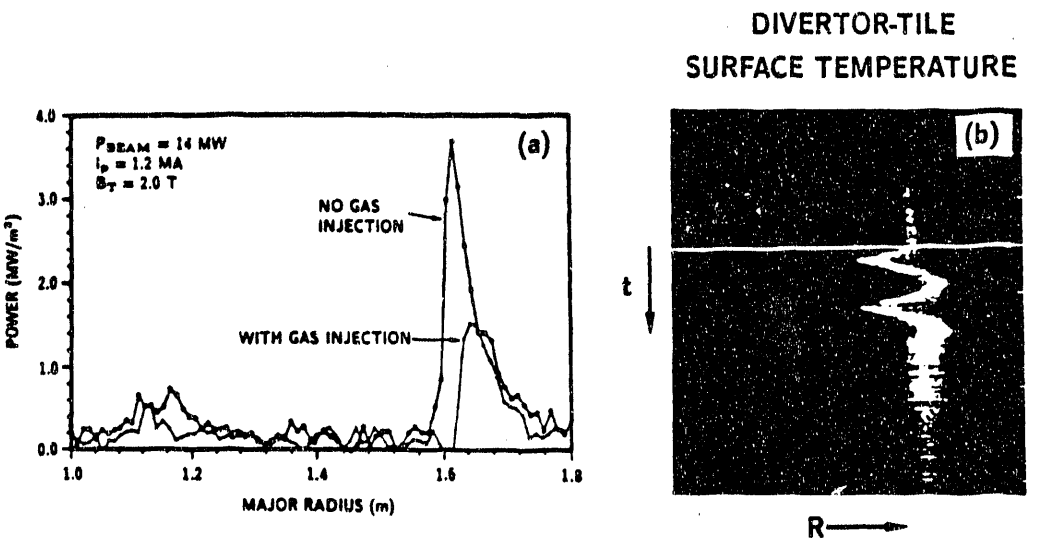

Fig. 9. (a) Heat fluxes across the single-null divertor target showing the reduction caused by deuterium gas injection between the separatrix strike points. (b) IR camera image of the outer separatrix strike point swept ±6 cm in major radius.

14. ELECTRON CYCLOTRON CURRENT DRIVE (ECCD)

The first step in the rf current drive program was taken with the observation of up to 70 kA of ECCD [16]. About 1.0 MW of 60 GHz rf power was launched in the fundamental X–mode from the high field side of DIII–D into discharges with Ohmic plasma current between 200 and 500 kA. These experiments were the first to be done in plasmas with strong single pass absorption (99%) and slowing down times for the current carrying superthermal electrons which are much shorter than the energy confinement time. Experiments were done with waves launched both with and against the plasma current. The loop voltage drops at constant current were compared to plasma resistivity changes using ONETWO. The bootstrap contribution was less than 10% of the total current. The loop voltage changes in excess of the resistive part give the black dot symbols in Fig. 10 for the experimentally determined driven current. The experimental I_{rf} exceeds that predicted by Fokker-Planck calculations with no remaining electric field (open circles). Fokker-Planck calculations estimating tail enhancement by the remaining electric field show this effect may account for the increased ECCD efficiency.

15. ADVANCED DIVERTOR PROGRAM (ADP)

A baffle and ring electrode structure has just been installed in DIII–D (Fig. 1). The outer leg of the separatrix can be rested on this ring and current driven into or drawn from the scrape-off layer from a power supply (600 V, 20 kA). This current can either aid or oppose the main plasma current. An increase in the edge plasma current density is expected to produce local second stability and so possibly to stabilize ELMs [31,37]. Outward cross-field transport in the scrape-off layer may be either increased or decreased depending on the sign of the applied $E_p \times B_T$ drift, perhaps affecting particle confinement or at least the scrape-off layer width [38]. Helicity injection current drive can be tested. The gas baffle between the ring and the wall enables divertor pumping experiments. Initially, studies of neutral pressure buildup will be made positioning the outer separatrix strike point either near or on the ring and puffing gas under the baffle. A cryo-pump to supply 50,000 l/sec under the baffle is being designed in collaboration with JET.

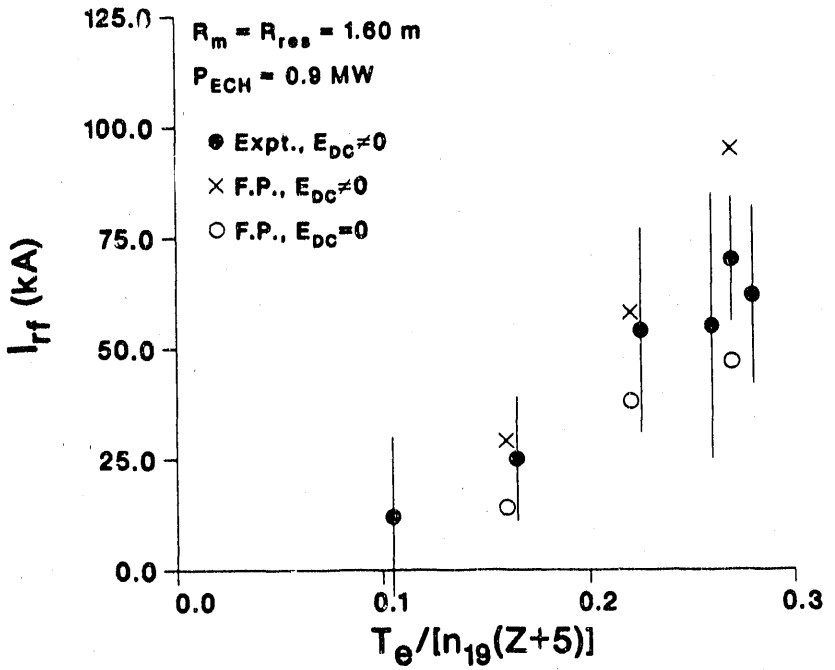

Fig. 10. Current driven by ECH measured (•) and Fokker-Planck predictions with (X) and without (o) electric field effects on the electron distribution function. $B_T =$ 2.1 T, 1×10^{19} m^{-3} $\leq \bar{n}_e \leq 2.5 \times 10^{19}$ m^{-3}, 200 kA $\leq I_p \leq$ 500 kA.

16. CONCLUSIONS

In high beta research the achieved beta values in divertor discharges have been pushed up to $\beta_T = 11\%$ in the low q regime and $\beta_p = 5.1$ ($\epsilon\beta_p = 1.8$) at high q. At intermediate q, β_N as high as 5 has been found stable and is theoretically expected to be stable for optimized profiles. The near term high leverage issue is to seek to establish whether the beta limit for optimized profiles rather generally lies at $\beta_N > 5$. Such a possibility would enhance prospects for current driven reactors operating at moderate to high q.

H–mode confinement in the high recycling open divertor geometry of DIII–D is about 1.7 times L–mode as represented by ITERP-89 scaling. Local transport studies favor a gyro-Bohm rather than the Bohm fundamental scaling prescription. In the hot ion H–mode regime, $T_i = 17$ keV has been reached and transport analysis reveals the principal improvement in H–mode from L–mode is a reduction of χ_e. DIII–D results favor the idea that the H–mode originates from a sudden increase in poloidal plasma flow at the edge, consistent with an increased negative E-field, and resulting in sufficient shear in the flow to stabilize turbulence. Sufficient

understanding of the physics and phenomenology of ELMs exists to utilize ELMs for impurity control, which has resulted in 10 second long H–mode and continuously declining impurity levels. Divertor X–point sweeping and radiation enhancement by both fuel and impurity gas puffed between the X–points have been shown able to lower peak divertor heat fluxes by factors of 3 and 2 respectively. Carbon blooms have not been observed in DIII–D despite local peak heat fluxes on the divertor tiles of 4 MW/m^2 and 50 MJ total heating energy injected. These results provide support for the effective use of H–mode in future devices and demonstrate that techniques are available to reduce divertor plate peak heat loads.

A clear observation of electron cyclotron current drive up to 70 kA has been made and is in accord with theory calculations. Methods of holding low density H–mode are being developed. The Advanced Divertor Program has installed a biasable ring and gas baffle structure for density control experiments. An in-vessel cryo-pump is being designed in collaboration with JET. Ion Bernstein wave heating did not produce central heating; only edge heating, parametric decay, and impurity influx were observed. The IBW antenna has been replaced with an ICRF fast wave current drive antenna as a first step toward full current drive by fast waves and EC waves with ECH (2 MW at 60 GHz and 2 MW at 110 GHz) used to produce the high temperatures needed for efficient current drive. An additional 5 MW, 110 GHz ECH system is being planned in cooperation with JAERI. An 8 MW ICRF fast wave system is also planned.

REFERENCES

[1] LAZARUS, E.A., LAO, L.L., OSBORNE, T.H., *et al.*, General Atomics report GA–A20265 (1990), submitted to Phys. Fluids.

[2] FERRON, J.R., CHU, M.S., HELTON, F.J., HOWL, W., KELLMAN, A.G., *et al.*, Phys. Fluids B **2** (1990) 1280.

[3] FERRON, J.R., CHU, M.S., HELTON, F.J., HOWL, W., KELLMAN, A.G., Controlled Fusion and Plasma Heating, Amsterdam 1990 (European Physical Society, 1990) 371.

[4] NAVRATIL, G.A., POLITZER, P.A., *et al.*, paper IAEA-CN-53/A-3-3, this conference.

[5] KIKUCHI, M., Nucl. Fusion **30** (1990) 265.

[6] SCHISSEL, D.P., BURRELL, K.H., DeBOO, J.C., GROEBNER, R.J., KELLMAN, A.G., *et al.*, Nucl. Fusion **29** (1989) 185.

[7] SCHISSEL, D.P., TUBBING, B.J.D., *et al.*, General Atomics report GA–A19925 (1990), accepted for publication in Nucl. Fusion.

[8] GROEBNER, R.J., BURRELL, K.H., and SERAYDARIAN, R.P., Phys. Rev. Lett. **64** (1990) 3015.

[9] SHAING, K.C., and CRUME, JR., E.C., Phys. Rev. Lett. **63** (1989) 2369.

10] BIGLARI, H., DIAMOND, P.H., and TERRY, P.W., Phys. Fluids B **2** (1990) 1.

[11] BURRELL, K.H., GROEBNER, R.J., CARLSTROM, T.N., KURKI-SUONIO, T., LOHR, J., *et al.*, Controlled Fusion and Plasma Heating, Amsterdam 1990 (European Physical Society, 1990) 271.

[12] WALTZ, R.E., DeBOO, J.C., and ROSENBLUTH, M.N., General Atomics report GA–A20172 (1990), submitted to Phys. Rev. Lett.

[13] ITER Team, "ITER Conceptual Design — Interim Report," IAEA, Vienna (1989).

[14] LUXON, J.L., *et al.*, to be published in Controlled Fusion and Plasma Heating, Amsterdam 1990 (European Physical Society, 1990).

[15] HILL, D.N., *et al.*, paper IAEA-CN–53/G-1-3, this conference.

[16] JAMES, R.A., GIRUZZI, G., FYARETDINOV, A., DeGENTILE, B., GORELOV, Y., *et al.*, Controlled Fusion and Plasma Heating, Amsterdam 1990 (European Physical Society, 1990) Part III, 1259.

[17] LUCE, T.C., JAMES, R.A., *et al.*, paper IAEA-CN-53/E-1-2, this conference.

[18] JACKSON, G.L., WINTER, J., LIPPMANN, S., PETRIE, T.W., DeBOO, J.C., *et al.*, in the Proceedings of the 9th International Conference on Plasma Surface Interactions in Controlled Fusion Devices, Bournemouth 1990.

[19] PINSKER, R.I., MAYBERRY, M.J., PORKOLAB, M., PRATER, R., in the Proceedings of the 8th Topical Conference on Radio-Frequency Power in Plasmas, Irvine, AIP (1989) 314.

[20] TROYON, F., GRUBER, R., SAURENMANN, H., SEMENZATO, S., and SUCCI, S., Plasma Phys. Control. Fusion **26** (1984) 209.

[21] LAO, L.L., STRAIT, E.J., TAYLOR, T.S., *et al.*, Plasma Physics Control. Fusion **31** (1989) 509.

[22] HOWL, W., TURNBULL, A.D., TAYLOR, T.S., *et al.*, General Atomics report GA–A19953 (1990), submitted to Phys. Fluids B.

[23] SYKES, A., TURNER, M.F., and PATEL, S., in Proceedings of the 11th European Conference on Controlled Fusion and Plasma Physics, Aachen (EPS, Petit-Lancy, Switzerland, 1983), Vol. II, p. 363.

[24] LAZARUS, E.A., TURNBULL, A.D., KELLMAN, A.G., FERRON, J.R., HELTON, F.J., *et al.*, Controlled Fusion and Plasma Heating, Amsterdam 1990 (European Physical Society, 1990) 427.

[25] SIMONEN, T.C., MATSUOKA, M., BHADRA, D.K., BURRELL, K.H., CALLIS, R.W., *et al.*, Phys. Rev. Lett. **61** (1988) 1720.

[26] MATSUMOTO, H., BURRELL, K.H., CARLSTROM, T.N., DOYLE, E.J., GOHIL, P., *et al.*, Controlled Fusion and Plasma Heating, Amsterdam 1990 (European Physical Society, 1990) 279.

[27] BURRELL, K.H., CARLSTROM, T.N., DOYLE, E.J., GOHIL, P., GROEBNER, R.J., *et al.*, Phys. Fluids B **2(6)** (1990) 1405.

[28] DOYLE, E.J., LEHECKA, T., LUHMANN, JR., N.C., PEEBLES, W.A., PHILIPONA, R., Controlled Fusion and Plasma Heating, Amsterdam 1990 (European Physical Society, 1990) Part I, 203.

[29] GROEBNER, R.J., PEEBLES, W.A., *et al.*, paper IAEA-CN-53/ A-6-4, this conference.

[30] OZEKI, T., CHU, M.S., LAO, L.L., TAYLOR, T.S., CHANCE, M.S., *et al.*, Nucl. Fusion **10** (1989) 1873.

[31] GOHIL, P., MAHDAVI, M.A., LAO, L., BURRELL, K.H., CHU, M.S., *et al.*, Phys. Rev. Lett. **61** (1988) 1603.

[32] BURRELL, K.H., *et al.*, Plasma Physics Control. Fusion **31** (1989) 1649.

[33] STOTT, P.E., DeBOO, J.C., PETRIE, T.W., St. JOHN, H., and SCHISSEL, D.P., Bull. Am. Phys. Soc. **34** (1989) 1940.

[34] CONTENT, D.A., MOOS, H.W., PERRY, M.E., BROOKS, N.H., and MAHDAVI, M.A., *et al.*, Nucl. Fusion **30** (1990) 701.

[35] ALLEN, S.L., RENSINK, M.E., *et al.*, J. Nucl. Mater. **162-164** (1989) 80.

[36] HILL, D.N., Bull. Am. Phys. Soc. **33** (1988) 1978.

[37] BISHOP, C.M., Nucl. Fusion **26** (1986) 1063.

[38] STAEBLER, G.H., and HINTON, F.L., Nucl. Fusion **29** (1989) 1820.

APPENDIX I
THE DIII-D TEAM
General Atomics, San Diego, California, U.S.A.

F.W. Baity,[a] H. Biglari,[b] G. Bramson, J.N. Brooks,[c] N.H. Brooks, D. Buchenauer,[d] K.H. Burrell, J.D. Callen,[e] R.W. Callis, T.N. Carlstrom, C. Challis,[f] M.S. Chance,[g] Z. Chang,[e] V. Chan, M.S. Chu, S. Coda,[h] A.P. Colleraine, J.C. DeBoo, J.C. De Gentile,[i] J. DeHaas,[j] P.H. Diamond,[b] I. Doi,[k] R. Dominguez, E.J. Doyle,[l] H. Duong,[m] R.F Ellis,[n] J.R. Ferron, T.K. Fowler,[o] R.L. Freeman, T. Fukuda,[p] A. Futch,[j] A. Fyaretdinov,[q] G. Giruzzi,[i] P. Gohil, Yu. Gorelov,[q] R. Goulding,[a] C.M. Greenfield, R.J. Groebner, G. Haas,[r] R. Harvey, W. Heidbrink,[i] D.N. Hill,[j] F.L. Hinton, D.J. Hoffman,[a] J. Hogan,[s] R. Hong, W. Howl, C.L. Hsieh, W.L. Hsu,[d] G.L. Jackson, R.A. James,[j] S. Janz,[n] T. Jarboe,[t] T. Jensen, R. Jong,[j] Y. Kamada,[p] A.G. Kellman, J. Kim, C.C. Klepper,[a] H. Kubo,[p] T. Kurki-Suonio,[o] L.L. Lao, R. La Haye, E.A. Lazarus,[a] R. Lee, T. Lehecka,[l] B. Leikind, S.I. Lippmann, J. Lister,[s] B. Lloyd,[u] J.M. Lohr, T.C. Luce, N.C. Luhmann, Jr.,[l] J.L. Luxon, M.A. Mahdavi, K. Matsuda, H. Matsumoto,[p] G. Matthews,[u] M. Mayberry, M. Menon,[a] B. Mills,[d] P. Mioduszewski,[a] C.P. Moeller, T. Ohkawa, T. Okazaki,[p] T.H. Osborne, D.O. Overskei, L. Owen,[a] W.A. Peebles,[l] P.I. Petersen, T.W. Petrie, C. Petty, R. Phillipona,[l] J. Phillips, R. Pinsker, P.A. Politzer, M. Porkolab,[g] G.D. Porter,[j] R. Prater, M.E. Rensink,[j] C. Rettig,[l] T. Rhodes,[l] J. Rodriguez,[i] M.N. Rosenbluth,[b] G. Sager,[v] M. Saigusa,[p] M.J. Schaffer, D.P. Schissel, L. Schmitz[l] J.T. Scoville, R.P. Seraydarian, T.C. Simonen, R.T. Snider, G.M. Staebler, B.W. Stallard,[j] R.D. Stambaugh, R. Stav, H. St. John, R.E. Stockdale, E.J. Strait, W. Tang,[g] P.L. Taylor, T.S. Taylor, P.K. Trost, V. Trukhin,[q] A. Turnbull, R. Waltz, J. Watkins,[w] J. Wight, J. Winter,[x] and D. Wroblewski[j]

PERMANENT ADDRESS

(a) Oak Ridge National Laboratory, USA
(b) University of California at San Diego, USA
(c) Argonne National Laboratory, USA
(d) Sandia National Laboratories, Livermore, USA
(e) University of Wisconsin, USA
(f) JET Joint Undertaking, EC
(g) Princeton Plasma Physics Labortory, USA
(h) Massachusetts Institute of Technology, USA
(i) Association EURATOM-CEA, Tore Supra, Cadarache, FR
(j) Lawrence Livermore National Laboratory, USA
(k) University of Campinas, BZ
(l) University of California at Los Angeles, USA
(m) University of California at Irvine, USA
(n) University of Maryland, USA
(o) University of California at Berkeley, USA
(p) Japan Atomic Energy Research Institute, JPN
(q) Kurchatov Institute, Moscow, USSR
(r) Max Planck Institute for Plasma Physics, Garching, FRG
(s) Ecole Polytechnique, Lausanne, SWTZ
(t) University of Washington, USA
(u) Culham Laboratory, UK
(v) University of Illinois, USA
(w) Sandia National Laboratories, Albuquerque, USA
(x) Institute of Plasmaphysics KFA, Jülich, FRG

END

DATE FILMED

02 / 05 / 91